Residual entropy and magnetocaloric effect in a diluted sawtooth spin model of hole-doped CuO chains

Miquéias J. Cirino[1], Onofre Rojas,[2] S. M. de Souza,[2] Jordana Torrico[3], Marcelo L. Lyra[1], and Maria S. S. Pereira[1]

[1]*Instituto de Física, Universidade Federal de Alagoas, 57072-970 Maceió-AL, Brazil*

[2]*Departamento de Física, Universidade Federal de Lavras, 37200-900 Lavras-MG, Brazil*

[3]*Departamento de Física, Universidade Federal de Minas Gerais, C.P. 702, 30123-970 Belo Horizonte-MG, Brazil*

Ground-state and magnetocaloric properties of a site-diluted sawtooth magnetic chain in the presence of an external magnetic field are exactly investigated by using the transfer-matrix method. The model captures the main magnetic interactions along CuO chains present in some hole-doped cuprates. The ground-state diagram is exhibited and analytical expressions for the residual entropy within each ground state and along the transition lines are derived. We explicitly discuss the role of the underlying pairing correlations and the entropy maximization principle. The isothermal entropy change is determined as a function of interaction parameters, doping concentration, and magnetic-field amplitude. Normal and inverse magnetocaloric effects are reported. Adiabatic demagnetization curves are discussed in connection with configurational and spin contributions to the residual entropy.

I. INTRODUCTION

Low-dimensional spin systems present intriguing electronic and magnetic properties that are not observed in analogous higher-dimensional systems [1]. Furthermore, due to their impressive structural variety, these materials have shown great potential in applications such as sensors and magnetic storage devices [2–4], spintronics [5,6], computation and quantum entanglement [7–11], in addition to applications in cooling processes [12–15]. In these systems, the competition between external fields and exchange interactions can induce a rich variety of phase transitions [16]. In fact the interplay between geometric frustration and quantum fluctuations in low-dimensional quantum magnets favors the generation of states with unconventional spin order, such as the spin liquid phase [17,18], different forms of nematic and multipolar order [19–21], the Haldane phase [22], as well as the existence of several disordered states.

Among the one-dimensional frustrated spin systems, special attention has been given to spin chains with interactions between first and second neighbors, also known as $J_1 - J_2$ models [19,23]. One of the most investigated topologies is the zigzag double chain, which can be understood as two chains connected by alternating ferro and antiferromagnetic couplings [24–26]. For zigzag $S = 1/2$ quantum spin chains with antiferromagnetic interactions between first and second neighbors $(J_1, J_2 < 0)$, it is well established that the ground state can undergo a transition from a gapless critical phase to a gaped phase at $(J_2/J_1)_c \simeq 0.241$ in the absence of a magnetic field, [19,27–29]. Furthermore, this system can exhibit plateaus on the magnetization curve and a chiral vector order in the presence of a magnetic field and anisotropic exchange interactions [30–33]. On the other hand, frustrated

ferromagnetic zigzag spin chains, with $J_1 > 0$ and $J_2 < 0$, received little attention until the discovery of superconductivity in organic conductors, especially in copper oxides [23,34,35].

Another largely investigated topology of $J_1 - J_2$ spin systems are the sawtooth chains. These systems have a rich variety of ground states [36,37]. Recently, theoretical and experimental studies showed that these systems can present a reentrance phenomenon of magnetic phases that can also be seen as an order-disorder effect [22,38,39]. Some conjectures have been made to understand this phenomenon, but frustration is taken as an essential ingredient [40]. In particular, such models are used to describe the magnetic properties of various cuprate superconducting ceramics, such as $SrCuO_2$, La_2CuO_4, $LiCuVO_4$, $Sr_2Cu_2Mo_3O_{12}$, and many others [19,34,35,41]. A large quantity of experimental evidence shows that the presence of oxygen hole-doping in CuO_2 planes, as well as CuO chains and ladders, plays an essential role in the phenomenon of superconductivity of these materials [42–46]. Cuprates also present other interesting aspects, such as metal-insulator transition, quantum critical points, and quantum antiferromagnetism in low dimensions [47,48]. On the other hand, the doping of electrons or holes in cuprates can be easily controlled. Therefore, it is possible to study the evolution of physical properties of these materials upon doping [49,50]. Indeed, impurities or small structural variations incorporated in the spin chains can significantly influence the ground state and, consequently, the physical properties of low-dimensional magnets [50–56].

In the last decades, research on semiconductors and diluted magnetic oxides has become an important branch of materials science [57]. This is due to successful demonstrations of the functionality of these materials in controlling magnetism through electric fields and electric currents [58,59],

magnetoresistance [60], and refrigeration applications [61–64]. In particular, systems where the frustration is induced by geometric factors and impurities have shown a pronounced magnetocaloric effect in the vicinity of transitions at finite fields, especially first-order transitions [65–67]. The magnetocaloric effect (MCE) consists of heating or cooling a magnetic material when subjected to a magnetic field [68,69]. Using the technique of adiabatic demagnetization, it is possible to build highly efficient ecological cooling devices over a wide temperature range [70]. Within this context, several theoretical and experimental studies have been carried out in the search for caloric materials with high performance [61,71,72]. Recently, a giant room-temperature magnetocaloric effect has been reported in transition-metal-based alloys on which the doping concentration plays a relevant role [73]. The description of this effect crucially relates to the dependence of the material's magnetic entropy on the temperature and applied magnetic field [65,74–76]. In conventional MCE, the magnetic entropy decreases when the external magnetic field increases isothermally. However, an inverse magnetocaloric effect has been observed in some frustrated ferrimagnetic systems in which the magnetic material cools when a magnetic field is applied in an adiabatic process with the magnetic entropy increasing under such conditions [77–80]. A significant inverse magnetocaloric effect can be achieved in the vicinity of quantum critical points due to enhanced quantum fluctuations [81]. Frustrated ferrimagnetic materials can also exhibit the phenomenon of magnetic compensation, where the total magnetization of the system is zero, but two or more sublattices can have nonzero magnetization at certain temperatures [82–84].

In the present work, we investigate the influence of doping on the magnetocaloric characteristics in a $S = 1/2$ antiferromagnetic spin chain. We consider that doping introduces a fraction of competing ferromagnetic decorated bonds. The model captures some aspects of the magnetic interactions in CuO chains present in some superconducting cuprate ceramics. Magnetic frustration and dilution can be sources of changes in the residual entropy and, therefore, directly impact the magnetocaloric properties. Using exact calculations, we report the ground-state diagram as a function of the external field and the exchange couplings ratio that acts as a relevant frustration parameter [25]. We also investigate the relationship between the ground-state residual entropy and the model's degree of doping. Finally, we compute the dependence of the entropy change on the magnetic field and temperature during the isothermal demagnetization process and discuss on the main physical ingredients affecting the adiabatic magnetocaloric cooling rate. We emphasize that the joint action of doping and magnetic frustration represents an efficient route to reach enhanced magnetocaloric refrigeration rates.

II. THE MODEL AND METHOD

We consider a spin chain model mimicking the main magnetic interactions found in alternating CuO chains present in several cuprate superconducting ceramics. In the absence of hole doping, the oxygen sites have no net spin and the copper sites have $S = 1/2$ spins that interact via a first-neighbor an-
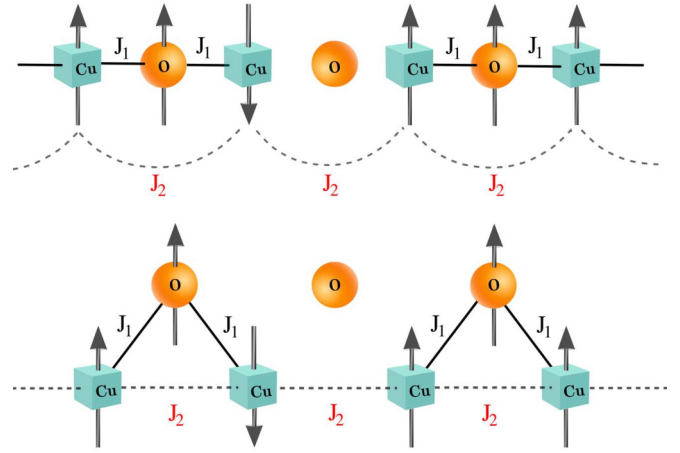

FIG. 1. (top panel) Diagrammatic representation of the randomly decorated spin model of a hole-doped CuO chain. The sites with Ising spins S_i (blue cubes) are all occupied by magnetic atoms and interact through an antiferromagnetic exchange coupling J_2. The oxygen sites (orange circles) are randomly occupied with a fraction p of Ising spins and interact with the nearest-neighbor S spins through a ferromagnetic coupling J_1. (bottom panel) The equivalent diluted sawtooth spin chain.

tiferromagnetic exchange coupling. Upon doping, a fraction p of the oxygen sites acquires a spin $1/2$ due to unpaired electrons that interact ferromagnetically with the neighboring copper spins. For simplicity, we will take these exchange couplings as Ising-like. The model can be seen as an antiferromagnetic $S = 1/2$ spin chain on which a fraction p of the bonds are randomly decorated by Ising spins interacting ferromagnetically with the nodal S spins. The above-described model is equivalent to a diluted sawtooth spin chain (see Fig. 1). The randomly decorated spin $1/2$ chain is described by the following cell Hamiltonian:

$$\mathcal{H}_i = -J_2 \sum_{i=1}^{N} S_i S_{i+1} - J_1 \sum_{i=1}^{N} \sigma_i (S_i + S_{i+1})$$
$$- H\left[\left(\frac{S_i + S_{i+1}}{2}\right) + \sigma_i\right] - \mu \sigma_i^2, \quad (1)$$

where $J_1 > 0$ represents the ferromagnetic exchange coupling between decorating and nodal spins while $J_2 < 0$ is the antiferromagnetic exchange coupling between nodal spins. $S_i = \pm 1$ accounts for the nodal Ising spins. $\sigma_i = \pm 1, 0$ represents the state of the decoration site ($\sigma_i = \pm 1$ describes the possible states of the decorating Ising spin and $\sigma_i = 0$ represents the absence of a decorating spin). The competition between these ferro and antiferromagnetic coupling gives rise to spin frustration. The random decoration is described by means of the parameter $\langle \sigma_i^2 \rangle$, which is the concentration of magnetic decorating spins per unit cell, namely, the decoration fraction p. μ is a chemical potential and H is an external magnetic field (units of $g\mu_B = 1$ are used). Here, μ_B is the Bohr magnetic moment. All magnetic ions are assumed to have the same gyromagnetic factor g. The full Hamiltonian of this model can be written as a sum of the cell Hamiltonians, $\mathcal{H}_{\text{total}} = \sum_i \mathcal{H}_i$.

The thermodynamic properties of the above randomly diluted sawtooth chain model can be obtained by the standard transfer-matrix technique. The grand-canonical partition function of the model under investigation can be written as follows:

$$\Xi_N = \sum_{\{S\}} \sum_{\{\sigma\}} \exp\{-\beta\mathcal{H}\}$$

$$= \sum_{\{S\}} \prod_{i=1}^{N} \mathrm{Tr}_i e^{-\beta\mathcal{H}_i} = \mathrm{Tr} W^N = \lambda_+^N + \lambda_-^N, \quad (2)$$

where $\beta = 1/(k_B T)$, k_B is the Boltzmann constant, T is the absolute temperature, and the summation $\sum_{\{S\}}$ is carried out over all possible S_i spin configurations. Here, Tr_i refers to the trace over the all degrees of freedom of spins and W is the transfer matrix,

$$W = \begin{pmatrix} \omega(1,1) & \omega(1,-1) \\ \omega(-1,1) & \omega(-1,-1) \end{pmatrix}, \quad (3)$$

where the individual matrix elements are given by

$$\omega(1,1) = e^{K_2+h}[1 + 2\nu \cosh(2K_1 + h)], \quad (4)$$

$$\omega(-1,-1) = e^{K_2-h}[1 + 2\nu \cosh(2K_1 - h)], \quad (5)$$

$$\omega(1,-1) = \omega(-1,1) = e^{-K_2}[1 + 2\nu \cosh(h)]. \quad (6)$$

Here, $K_1 = \beta J_1$, $K_2 = \beta J_2$, $h = \beta H$, and $\nu = e^{\beta\mu}$. In the thermodynamic limit $N \to \infty$, only the largest eigenvalue λ_+ effectively contributes to the partition function and all thermodynamic averages can be calculated from the eigenvalues and eigenvectors of the transfer matrix (3). In the present problem, it is more convenient to use the decoration fraction as a control parameter instead of the chemical potential. Thus, the fraction of decorated bonds is given by

$$p = \langle \sigma_i^2 \rangle = \frac{\nu}{\lambda_+} \frac{\partial \lambda_+}{\partial \nu}. \quad (7)$$

All other thermodynamic quantities can be directly computed using standard statistical mechanics relations. In particular, the Helmholtz free energy per unit cell can be written as $\mathcal{F} = -T \ln \lambda_+ + T p \ln \nu$. The residual entropy per cell at $T = 0$ depends only on the fraction of occupied σ sites and can be exactly calculated as $S = \frac{1}{N} k_B \ln \Omega$, where Ω is the number of the accessible states of the spin chain in the ground state. For the analysis of the magnetocaloric effect it is crucial to know the dependence of the magnetic entropy on the temperature and magnetic field. In fact, the MCE can be characterized by the entropy change $\Delta S_T = S(T, H) - S(T, H = 0)$ in the process of isothermal demagnetization. In present convention, the negative values of the $\Delta S_T < 0$ corresponds to normal MCE while positive values of the $\Delta S_T > 0$ denotes inverse MCE [85].

III. RESULTS AND DISCUSSION

A. Ground-state diagram

The Hamiltonian model (1) can be exactly solved and the ground-state energies obtained as a function of the external

TABLE I. Energies per unit cell of all available ground states of the diluted sawtooth model: the saturated ferromagnetic state F-F, the antiferro-ferromagnetic state AFM-F, and the antiferromagnetic frustrated state AFM-Fr.

	E
F-F	$p(-2J_1 - J_2 - 2H - \mu) + (1-p)(-J_2 - H)$
AFM-F	$p(-2J_1 - J_2 - 2H - \mu) + (1-p)J_2$
AFM-Fr	$p(J_2 - H - \mu) + (1-p)J_2$

field h and exchange coupling constants J_1 and J_2. We identified that there are three possible ground states depending on the set of model parameters: A saturated ferromagnetic ground state (F-F) with all spins aligned in the external field direction; an antiferro-ferromagnetic phase (AFM-F) in which the spins S_i are aligned antiparallel to each other in the absence of a decorating magnetic ion. However, the spins S_i are aligned parallel to the field when a decorating spin is present. The third possible ground state is an antiferromagnetic frustrated state (AFM-Fr) with the spins S_i aligned antiparallel to each other in both the absence and presence of a decorating spin. In this last phase, the spins in the decorating sites are aligned to the field direction but assume random orientations in the absence of an external field.

The energies per unit cell for these possible states are given in Table I. Notice that, in the limit where there are only cells with interstitial sites occupied by magnetic ions ($p \to 1$), the phases F-F and AFM-F are equivalent. The transition line is given by the condition $\tilde{E}_{\text{F-F}} = \tilde{E}_{\text{AFM-F}}$. On the other hand, the AFM-F and AFM-Fr states are equivalent when all decorating sites are empty ($p \to 0$). In Fig. 2, we show the typical ground-state diagram in J_2/J_1-H/J_1 parameter space. The diagram exhibits three possible ground states. For large magnetic fields, the saturated ferromagnetic state (F-F) predominates whenever $H/|J_1| > -2J_2/|J_1|$. Otherwise, the AFM-F state sets up. At very low fields, the AFM-Fr ground state takes place in the regime of large values of the ratio between the exchange couplings. The transition line corresponds to $E_{\text{AFM-F}} = E_{\text{AFM-Fr}}$. At zero field, the AFM-Fr state emerges
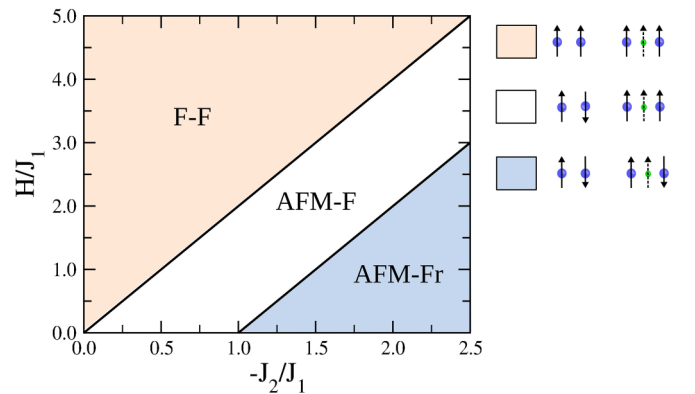

FIG. 2. Ground-state diagram in the external field H/J_1 versus ratio between exchange couplings $-J_2/J_1$ plane. The transitions lines can be obtained by comparing the energies per unit cell of each phase. We sketch the unit-cell configuration for the three possible ground states. $g\mu_B = 1$ units were used.

TABLE II. Entropy per unit cell S/k_B for all states and transition lines appearing in the ground-state diagram Fig. 2. Here, p is the fraction of occupied σ sites, $q = [5 - 4p - (5 - 4p^2)^{1/2}]/10$ and $\epsilon = (\frac{p-\epsilon}{2})\sqrt{(1+\epsilon)/(1-\epsilon)}$. From the latter, one can write $p = \epsilon[2\sqrt{(1-\epsilon)/(1+\epsilon)} + 1]$.

Ground state	Entropy (S/k_B)
F-F; (AFM-F)$_{H=0}$; (AFM-Fr)$_{H\neq0}$	$-p \ln p - (1-p)\ln(1-p)$
(AFM-Fr)$_{H=0}$	$-p \ln p - (1-p)\ln(1-p) + p \ln 2$
(AFM-F)$_{H\neq0}$	$-p \ln p + (\frac{1+p}{2})\ln(\frac{1+p}{2}) - (\frac{1-p}{2})\ln(\frac{1-p}{2})$
Transition lines	Entropy (S/k_B)
F-F $\rightarrow$ AFM-F	$-p \ln(p) + (\frac{1+p}{2})\ln(1-q) - (\frac{1-p}{2})\ln(q)$
(AFM-F $\rightarrow$ AF-Fr)$_{H\neq0}$	$(\frac{1+\epsilon}{2})\ln(1+\epsilon) + (\frac{1-\epsilon}{2})\ln(1-\epsilon) - \epsilon \ln(2\epsilon) - (1-p)\ln(1-p) - (p-\epsilon)\ln(p-\epsilon)$
(AFM-F $\rightarrow$ AF-Fr)$_{H=0}$	$-p \ln(p) - (1-p)\ln(1-p) + p \ln(3)$

for $-J_2/J_1 > 1$. At zero field, the average cell magnetization vanishes for all ground states. For finite magnetic fields with a fraction p of decorated cells and $(1-p)$ of nondecorated cells, the average cell magnetization $m = \langle S_i + \sigma_i \rangle$ of the nondegenerate ground states is given by

$$m_{\text{F-F}} = 1 + p,$$
$$m_{\text{AFM-F}} = 2p,$$
$$m_{\text{AFM-Fr}} = p. \qquad (8)$$

B. Residual entropy

Associated with the annealed random character of the doping, the ground states sustain residual entropies. These can be extracted as the zero-temperature limits of the entropy calculated directly from the free energy. The main features of the finite-temperature entropy derived from the free energy will be detailed in the next section to explore the magnetocaloric effect. In this section, we provide an alternative calculation of the zero-temperature entropies based in the direct combinatorial calculation of the residual number of states to explicitly discriminate the contributions coming from the bond configurational degrees of freedom associated with the random dilution and the spin degrees of freedom resulting from the competing magnetic interaction [86]. In the F-F, (AF-F)$_{H=0}$, and (AF-Fr)$_{H\neq0}$ states, the residual entropy can be directly computed by considering that the unit cells with and without a decorating spin are randomly and independently distributed. In this scenario the number of possible configuration is just

$$\Omega = \frac{N!}{(pN)![(1-p)N]!}, \qquad (9)$$

from which the residual entropy per unit cell $S = \frac{1}{N}k_B \ln \Omega$ follows. In the absence of an external field, the (AF-Fr)$_{H=0}$ depicts an additional contribution due to the random orientation of the decorating spin.

Special attention has to be driven to compute the residual entropy in the (AF-F)$_{H\neq0}$ ground state. In this case, the unit cells without the decorating spin combine in pairs due to their antiferromagnetic ordering. Therefore, the system is effectively composed of $(1-p)N/2$ pairs of cells without a decorating spin and pN cells with a decorating spin. The total number of elements to be randomly and uncorrelated dis-

tributed is $N_e = [p + (1-p)/2]N = (1+p)N/2$. Therefore, the total number of possible configurations is

$$\Omega = \frac{N_e!}{(pN)![(1-p)N/2]!}. \qquad (10)$$

The resulting expressions for the residual entropies in the above ground states are summarized in Table II. Along the transition lines, there are additional contributions to the residual entropies due to degeneracy. In the F-F to AFM-F transition line, the $(1-p)N$ unit cells without a decorating spin can be either with the spins aligned parallel or antiparallel to each other. The system is therefore composed of a random distribution of three distinct elements: pN cells with decorating spins ferromagnetically aligned, κN nondecorated cells with ferromagnetically aligned spins, and qN pairs of nondecorated cells with antiferromagnetically aligned spins. Here, $(1-p)N = \kappa N + 2qN$. The total number of elements to be distributed is $N_e = pN + \kappa N + qN = (1-q)N$, with the number of possible configurations being given by

$$\Omega = \frac{N_e!}{(pN)!(\kappa N)!(qN)!}. \qquad (11)$$

To determine the fraction of paired cells, we explore the maximum entropy principle which provides the optimal value of q as an explicit nonlinear function of p (see Table II). Accordingly, the average cell magnetization along this transition line acquires a nonlinear dependence on p, being given by $m_{\text{F-F to AFM-F}} = 1 + p - 2q$.

Along the AFM-F to AFM-Fr transition line, the cells can also be found in three distinct configurations. Among the pN decorated cells, a number $(p-\epsilon)N$ have nodal spins antiferromagnetically aligned while the remaining ϵN cells are in the ferromagnetic configuration. All $(1-p)N$ nondecorated cells are in the antiferromagnetic state. The antiferromagnetic cells combine in pairs in the presence of an external magnetic field. The total number of pairs is $(1-\epsilon)N/2$ and the total number of elements including unpaired and paired cells is $N_e = (1+\epsilon)N/2$. Furthermore, there are several ways to form pairs using either decorated or nondecorated cells. Accordingly, the total number of possible configurations of the system is given by

$$\Omega = \frac{N_e!}{[\epsilon N]![(1-\epsilon)N/2]!} \frac{[(1-\epsilon)N]!}{[(1-p)N]![(p-\epsilon)N]!}, \qquad (12)$$
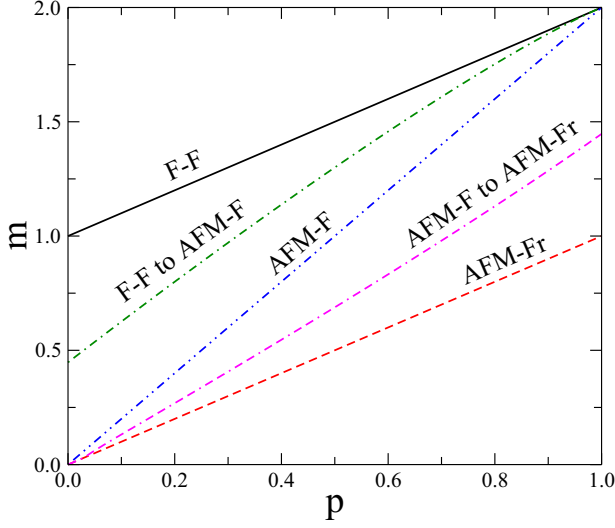
FIG. 3. Cell magnetization $m = \langle S_i + \sigma_i \rangle$ at finite magnetic fields as a function of the fraction p of decorated cells for all three possible ground states F-F, AFM-F, and AFM-Fr and along the two transition lines. Notice the nonlinear dependence at the transitions on which $q(p) = (m_{\text{F-F}} - m_{\text{F-F to AFM-F}})/2$ and $\epsilon(p) = m_{\text{AFM-F to AFM-Fr}} - m_{\text{AFM-Fr}}$.

where the first fraction corresponds to the total number of possible permutations of unpaired and paired cells and the second fraction accounts for the total number of distinct ways to form paired cells. Here, we also need the consider the principle of maximum entropy to determine the optimal distribution of decorated cells in the ferro and antiferromagnetic configurations. The optimal value of α is found to depend on p according to the self-consistence expression given in Table II. An explicit $\epsilon(p)$ can be obtained as a solution of the resulting third-order polynomial. However, the resulting algebraic expression (not shown) is quite cumbersome and does not bring any new insight. Alternatively, an explicit form $p(\epsilon)$ can be extracted which is useful to analyze limiting cases. Along this transition line $m_{\text{AFM-F to AFM-Fr}} = p + \epsilon$. The cell magnetization curves in function of the decoration fraction p for all three ground states and along the two transition lines are shown in Fig. 3.

In the zero-field transition point between the AFM-F and AFM-Fr ground states, there is no pair correlations among the antiferromagnetic cells. Furthermore, the decorating spin in the antiferromagnetic configuration can be equally found in either one of the two possible states. Therefore, the total number of possible configurations is

$$\Omega = \frac{N!}{(\alpha N)![(p - \alpha)N]![(1 - p)N]!} 2^{\alpha N}, \qquad (13)$$

with $\alpha = 2p/3$ corresponding to the maximum entropy condition. The resulting entropy in this zero-field transition point is also included in Table II.

In Fig. 4 we plot the entropy per unit cell as function of the decorating fraction p for all possible ground-state configurations. In Fig. 4(a) we show the zero-field case. Within the AFM-F phase ($J_2/J_1 = -0.5$) the entropy is just due to the uncorrelated distribution of decorated and nondecorated
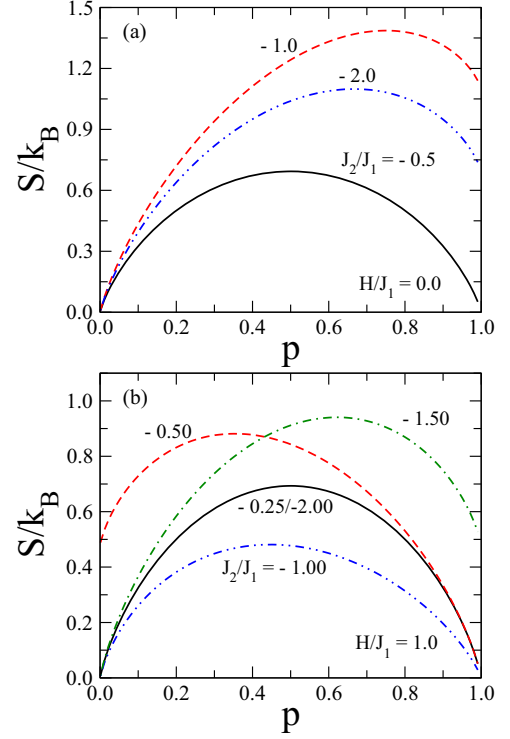

FIG. 4. Entropy per unit cell as a function of the degree of dilution for two representative values of the magnetic field and different values of the ratio between exchange couplings J_2/J_1. (a) $H/J_1 = 0$ and (b) $H/J_1 = 1.0$.

cells. It vanishes in both $p = 0$ and $p = 1$ limits, with a maximum $S/k_B = \ln 2$ at $p = 1/2$. Within the AFM-Fr ground state ($J_2/J_1 = -2.0$), there is an additional contribution coming from the degenerate orientation of the decorating spins. The entropy develops an asymmetric dependence on p with $S/k_B = \ln 2$ at $p = 1$ and a maximum entropy $S/k_B = \ln 3$ at $p = 2/3$. In the transition point ($J_2/J_1 = -1$), another contribution to the entropy comes from the two possible ferro and antiferromagnetic configurations of the decorated cells. This results in a maximum entropy $S/k_B = \ln 4$ at $p = 3/4$ as well as $S/k_B = \ln 3$ at $p = 1$.

In Fig. 4(b) we show the entropy curves at finite magnetic fields. Within the F-F and AFM-Fr ground states, $J_2/J_1 = -0.25$ and -2.0, respectively, and the residual entropy is just due to the random distribution of decorated and nondecorated cells. Within the AFM-F ground state the pairing correlations of the nondecorated cell reduces the entropy. The curve becomes asymmetric with maximum entropy $S/k_B = \ln[(\sqrt{5} + 1)/2] \simeq 0.4812 k_B$ at $p = \sqrt{5}/5$ (dashed-dot-dotted line). At the transition lines, the competition between the pairing correlation and the cell configuration degeneracy results in an overall increase of the residual entropy. At the F-F to AFM-F transition and $p = 0$, the fraction of paired nondecorated antiferromagnetically aligned cells is $q = (5 - \sqrt{5})/10$, giving up to a residual entropy $S/k_B = \ln[(\sqrt{5} + 1)/2] \simeq 0.4812$. An equivalent residual entropy persists in the AFM-F to AFM-Fr transition point at $p = 1$ with a fraction $(\epsilon - \sqrt{5})/5$ of antiferromagnetically aligned
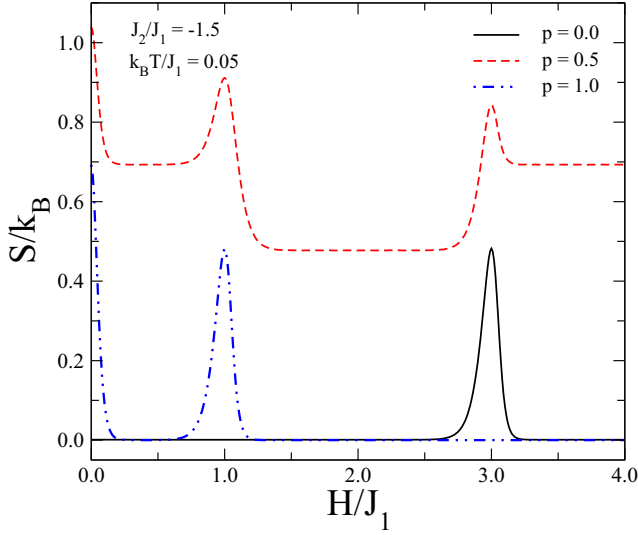
FIG. 5. Field dependence of the entropy per unit cell for three representative values of the degree of dilution p. Here we use $J_2/J_1 = -1.5$ for which the zero-temperature ground state is antiferromagnetic frustrated state AFM-Fr.
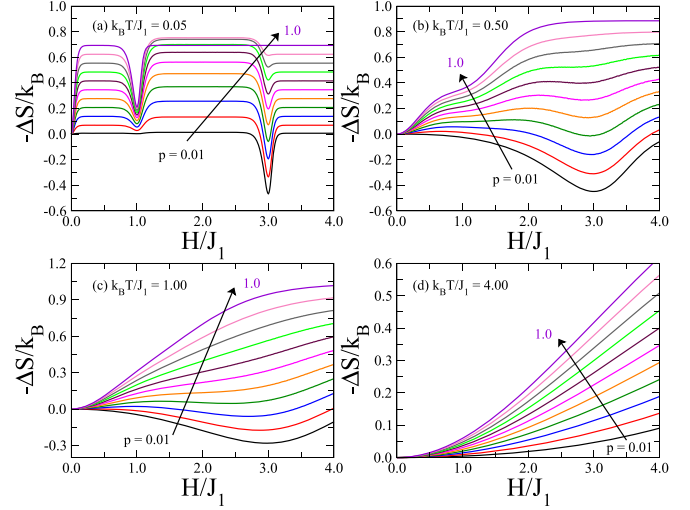

FIG. 6. Isothermal entropy change $-\Delta S/k_B = -[S(T, H) - S(T, 0)]/k_B$ as a function of the magnetic field for representative values of the temperature. The arrow indicates the increase in the degree of dilution p. Here we use $J_2/J_1 = -1.5$.

decorated cells. Maximum residual entropy at the transition lines is developed at intermediate decoration fractions.

IV. MAGNETOCALORIC ENTROPY CHANGE AND ISOENTROPIC CURVES

In this section we report the main behavior of the entropy at finite temperatures. It can be also exactly computed from the largest eigenvalue λ_+ of the transfer matrix given in Sec. II. In brief, one starts by using Eq. (7) to obtain the chemical potential for a given set of thermodynamic variables (T, H, p) in order to consider conditions of fixed temperature, magnetic field, and fraction of decorated bonds. The finite-temperature entropy per bond is just extracted from the thermodynamic relation $S = -\partial \mathcal{F}/\partial T|_{H,p}$ where the chemical potential is eliminated from the Helmholtz free-energy expression in favor of the decorating fraction.

Before analyzing the main characteristics associated with the magnetocaloric entropy changes, we emphasize the low-temperature behavior of the entropy as a function of the external magnetic field and decorating fraction, as shown in Fig. 5 for the illustrative case of $J_2/J_1 = -1.5$. In the limit $p = 0$, i.e., in the absence of decorating spins, the ground state is nondegenerate except at the transition field $H/J_1 = 3.0$ at which the nondecorated cells have two degenerate configurations. Therefore, the low-temperature entropy is roughly null, developing a narrow peak at the transition field. All cells are decorated in the opposite limit of $p = 1$. Therefore, only the transition occurring at $H/J_1 = 1.0$ is signaled by a narrow peak in the entropy representing the degenerate configurations of the decorated cells. Notice that a second narrow peak is present at $H = 0$ due to the additional degeneracy of the decorating spin in the absence of a magnetic field. All the above described peaks are signaled at intermediate dilution fractions. Besides these entropy contributions due to degenerate cell configurations, there are additional entropy

contributions associated with the random nature of the distribution of decorated and nondecorated cells. These appear as entropy plateaus. The entropy plateaus at the F-F and AFM-Fr ground states are equivalent. The lower plateau in the AFM-F ground state results from the underlying pairing correlations.

In Fig. 6 we show the magnetocaloric entropy change $-\Delta S$ as a function of the magnetic field for distinct temperatures and decorating fractions. Notice that normal MCE ($-\Delta S > 0$) predominates at high temperatures, with larger entropy changes for larger values of p for which the high-temperature entropy has the additional contribution of the decorating spins. The magnetocaloric entropy change exhibits new features at low temperatures. At first, one notices that an inverse MCE ($-\Delta S < 0$) appears in the vicinity of the upper critical field $H/J_1 = 3.0$, especially at low decorating fractions. The inverse MCE is more pronounced at low temperatures, although becoming restrictive to a narrower range of magnetic fields. On the other hand, normal MCE depicts plateaus at low temperatures, being strongly suppressed in the vicinity of the lower critical field $H/J_1 = 1.0$. The above features of the magnetocaloric entropy change can also be identified in Fig. 7 where we plot its temperature dependence for some characteristic magnetic fields. It evinces that normal MCE predominates, except in the low-temperature regime for small decorating fractions and in the vicinity of the upper critical field. The inverse MCE results from the strong degeneracy at the upper critical field, in contrast with the ordered zero-field ground state.

The complete temperature and magnetic-field dependence of the entropy is shown in Fig. 8 for two representative values of J_2/J_1. Figure 8(a) corresponds to $J_2/J_1 = -0.5$ for which one has the AFM-F zero-field ground state and just the field-induced transition to the F-F ground state takes place. The AFM-F zero-field ground state has a configurational residual entropy due to the random distribution of decorated and nondecorated cells. Therefore, large isoentropic refrigeration rates $\partial T/\partial H|_S$ are obtained in the regime of low-temperatures
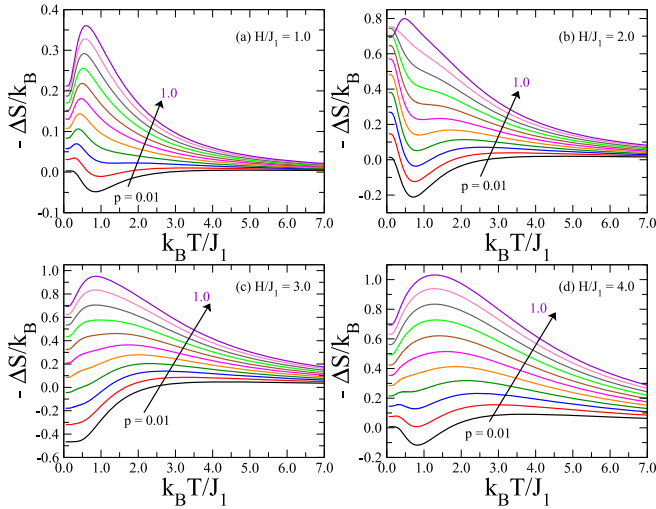
FIG. 7. Isothermal entropy change $-\Delta S/k_B$ as a function of temperature for fixed external magnetic-field amplitude. The arrow indicates increasing degree of dilution p. Here we use $J_2/J_1 = -1.5$.

both in the vicinity of the critical field as well in the low-field regime. Adiabatic magnetic refrigeration down to $T = 0$ can be obtained for any initial condition below the dashed line corresponding to $S(T = 0, H = 0)$. Figure 8(b) shows the case of a larger antiferromagnetic coupling $J_2/J_1 = -1.5$. In this case, the zero-field ground state is AFM-Fr that has residual entropy coming from both configurational and spin contributions. Here, large isoentropic refrigeration rates are achieved in the vicinity of the two critical fields as well as near zero field. It is important to stress that the isoentropic curves that reaches $T = 0$ at low fields span a wider range of temperatures when compared with the previous case.

V. SUMMARY AND CONCLUSIONS

In summary, we exactly solved a spin chain model having a fraction p of decorated unit cells with ferromagnetic Ising coupling between decorating and nodal spins and a fraction $(1 - p)$ of direct antiferromagnetic Ising coupling between nodal spins. The model mimics the main magnetic interactions along CuO spin chains present in a class of doped copper-oxide superconducting ceramics.

We obtained the exact ground-state diagram and provided analytical expressions for the residual entropy within each ground state and along the transition lines. We discussed in detail the role played by pairing correlations among cells with antiferromagnetically aligned nodal spins. Furthermore, we showed that the maximum entropy principle needs to be invoked to properly account for the residual entropy at the degenerate transition lines. The dependence of the residual entropy on the doping fraction in each one of the relevant ground states was reported.

Furthermore, using the grand-canonical ensemble framework, we computed the thermal entropy and explored the isothermal magnetocaloric entropy change as a function of the external magnetic field and temperature, evincing the physical conditions required to reach normal and inverse MCE. Finally, we showed that large adiabatic magnetic refrigeration
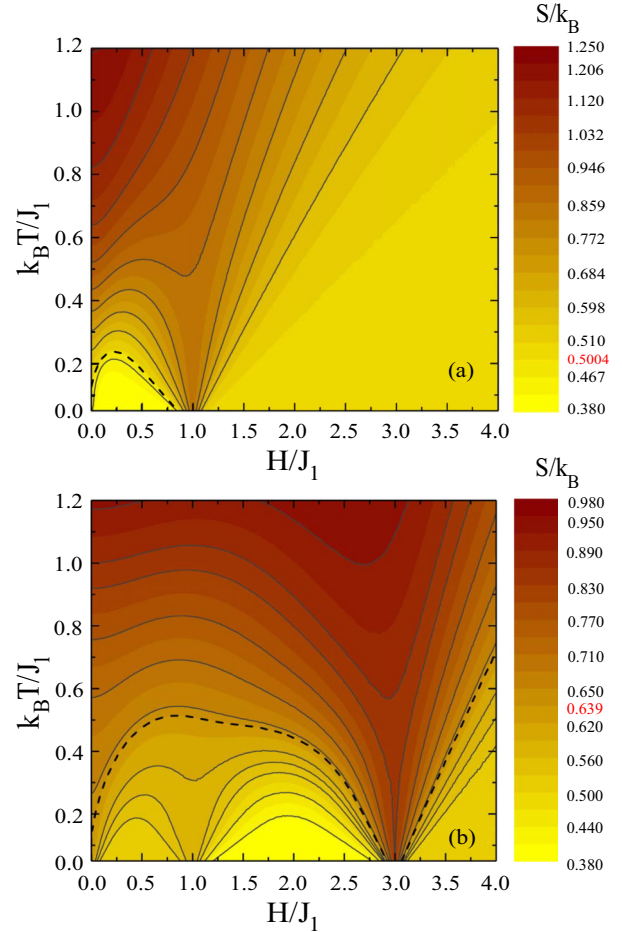

FIG. 8. Entropy density plot evincing curves of isoentropy for the particular case of decoration degree $p = 0.2$. (a) $J_2/J_1 = -0.5$ for which the zero-field ground state is AFM-F. A single critical field is observed. Dashed line corresponds to $s(T, H)/k_B = s(0, 0)/k_B = 0.5004 \cdots$. (b) $J_2/J_1 = -1.5$ for which the zero-field ground state is AFM-Fr. This case presents two critical fields. Dashed line corresponds to $s(T, H)/k_B = s(0, 0)/k_B = 0.639 \cdots$. Notice that maxima adiabatic cooling rates take place near $H = 0$ as well as near the critical magnetic fields.

rates can be reached in the vicinity of the critical magnetic fields, particularly in the presence of spin frustration for which the ground-state entropy has contributions from both configurational cell disorder and spin degeneracy. In this case, large adiabatic magnetic refrigeration rates are found at low temperatures and magnetic fields, an ideal scenario for the development of magnetic cooling cycles. In particular, larger magnetocaloric rates are achieved when the residual entropy at zero temperature and magnetic field becomes larger. Our results evidence the advantage in considering simultaneously magnetic frustration and dilution. In the frustrated phase, the residual entropy raises from $S = k_B \ln 2$ in the absence of dilution to $S = k_B \ln 3$ at an ideal dilution fraction $p = 2/3$. At the critical point delimiting the transition between the frustrated and nonfrustrated phases, the residual entropy due just to the spin degeneracy increases to $S = k_B \ln 3$. In this case, dilution can also improve the residual entropy which reaches a maximum $S = k_B \ln 4$ at $p = 3/4$. Even in the non-

frustrated phase that has no residual entropy in the absence of dilution, a maximum of $S = k_B \ln 2$ is reached at $p = 1/2$ [see discussion of Fig. 4(a)]. Accordingly, dilution can improve the refrigeration rate irrespective to the ground-state order of the pure system. An additional advantage of dilution is that the corresponding fraction can be controlled in the synthesis of the magnetic compound through the doping fraction, thus making it reliable to tune the dilution fraction on the desired optimal values.

It would be interesting to extend the present analysis to other low-dimensional frustrated spin structures usually found in doped copper-oxide ceramics such as CuO_2 spin chains, ladders and planes. These would provide a more complete picture related to the capability of using this class of ceramic materials to perform magnetic refrigeration processes. The present study detailed the significant role played by doping to reach large magnetocaloric rates, a feature consistent with recent experimental findings on transition-metal alloys [62,73]. Future extensions to include the full Heisenberg character

of the magnetic interaction would be in order because the joint effect of dilution, magnetic frustration, and quantum fluctuations signals to a class of highly effective systems for magnetic cryogenic applications [81]. However, advanced numerical methods such as the density-matrix renormalization group and quantum Monte Carlo simulations would be required to deal with the resulting Hamiltonian system. The analytical results reported here can be used to probe the accuracy of these numerical methods in the limit of reduced quantum fluctuations.

[1] T. Giamarchi, *Quantum Physics in One Dimension* (Clarendon Press, Oxford, 2003).

[2] C. Wurm, M. Morcrette, G. Rousse, L. Dupont, and C. Masquelier, Chem. Mater. **14**, 2701 (2002).

[3] Y. Uebou, S. Okada, M. Egashira, and J.-I. Yamaki, Solid State Ionics **148**, 323 (2002).

[4] Y. Wang, J. Li, and D. Viehland, Mater. Today **17**, 269 (2014).

[5] V. Garcia, M. Bibes, L. Bocher, S. Valencia, F. Kronast, A. Crassous, X. Moya, S. Enouz-Vedrenne, A. Gloter, D. Imhoff, C. Deranlot, N. D. Mathur, S. Fusil, K. Bouzehouane, and A. Barthélémy, Science **327**, 1106 (2010).

[6] H. Ohno, Nat. Mater. **9**, 952 (2010).

[7] N. S. Ananikian, L. N. Ananikyan, L. A. Chakhmakhchyan, and O. Rojas, J. Phys.: Condens. Matter **24**, 256001 (2012).

[8] M. Rojas, S. M. de Souza, and O. Rojas, Phys. Rev. A **89**, 032336 (2014).

[9] J. Torrico, M. Rojas, M. S. S. Pereira, J. Strečka, and M. L. Lyra, Phys. Rev. B **93**, 014428 (2016).

[10] F. Souza, L. M. Veríssimo, J. Strečka, M. L. Lyra, and M. S. S. Pereira, Phys. Rev. B **102**, 064414 (2020).

[11] F. Souza, G. M. A. Almeida, M. L. Lyra, and M. S. S. Pereira, Phys. Rev. A **102**, 032421 (2020).

[12] I. Takeuchi, and K. Sandeman, Phys. Today **68**, 48 (2015).

[13] S. Crossley, N. D. Mathur, and X. Moya, AIP Adv. **5**, 067153 (2015).

[14] K. Szałowski and T. Balcerzak, Sci. Rep. **8**, 5116 (2018).

[15] H. Čenčariková, and J. Strečka, Phys. Rev. E **98**, 062129 (2018).

[16] M. Takigawa and F. Mila, in *Introduction to Frustrated Magnetism: Materials, Experiments, Theory*, edited by C. Lacroix, P. Mendels, and F. Mila (Springer, New York, 2011), Vol. 164.

[17] L. Balents, Nature (London) **464**, 199 (2010).

[18] J. Knolle and R. Moessner, Annu. Rev. Condens. Matter Phys. **10**, 451 (2019).

[19] T. Hikihara, L. Kecke, T. Momoi, and A. Furusaki, Phys. Rev. B **78**, 144404 (2008).

[20] J. Sudan, A. Lüscher, and A. M. Läuchli, Phys. Rev. B **80**, 140402(R) (2009).

[21] H.-K. Jin, A. Pizzi, and J. Knolle, Phys. Rev. B **106**, 144312 (2022).

[22] Y. Yang, S.-J. Ran, X. Chen, Z.-Z. Sun, S.-S. Gong, Z. Wang, and G. Su, Phys. Rev. B **101**, 045133 (2020).

[23] F. Heidrich-Meisner, A. Honecker, and T. Vekua, Phys. Rev. B **74**, 020403(R) (2006).

[24] U. Schwingenschlögl, Phys. Rev. B **75**, 212408 (2007).

[25] A. K. Kolezhuk, F. Heidrich-Meisner, S. Greschner, and T. Vekua, Phys. Rev. B **85**, 064420 (2012).

[26] I. T. Shyiko, I. P. McCulloch, J. V. Gumenjuk-Sichevska, and A. K. Kolezhuk, Phys. Rev. B **88**, 014403 (2013).

[27] F. D. M. Haldane, Phys. Rev. B **25**, 4925 (1982).

[28] S. R. White and I. Affleck, Phys. Rev. B **54**, 9862 (1996).

[29] L. Capriotti, F. Becca, S. Sorella, and A. Parola, Phys. Rev. B **67**, 172404 (2003).

[30] T. Hikihara, M. Kaburagi, and H. Kawamura, Phys. Rev. B **63**, 174430 (2001).

[31] K. Okunishi and T. Tonegawa, Phys. Rev. B **68**, 224422 (2003).

[32] A. Kolezhuk and T. Vekua, Phys. Rev. B **72**, 094424 (2005).

[33] I. P. McCulloch, R. Kube, M. Kurz, A. Kleine, U. Schollwöck, and A. K. Kolezhuk, Phys. Rev. B **77**, 094404 (2008).

[34] M. Hase, H. Kuroe, K. Ozawa, O. Suzuki, H. Kitazawa, G. Kido, and T. Sekine, Phys. Rev. B **70**, 104426 (2004).

[35] M. Enderle, C. Mukherjee, B. Fåk, R. K. Kremer, J.-M. Broto, H. Rosner, S.-L. Drechsler, J. Richter, J. Malek, A. Prokofiev, W. Assmus, S. Pujol, J.-L. Raggazzoni, H. Rakoto, M. Rheinstädter, and H. M. Rønnow, Europhys. Lett. **70**, 237 (2005).

[36] W. L. Queen, S.-J. Hwu, and L. Wang, Angew. Chem. Int. Ed. **46**, 5344 (2007).

[37] J. P. West, S.-J. Hwu, and W. L. Queen, Inorg. Chem. **48**, 8439 (2009).

[38] V. O. Garlea, L. D. Sanjeewa, M. A. McGuire, P. Kumar, D. Sulejmanovic, J. He, and S.-J. Hwu, Phys. Rev. B **89**, 014426 (2014).

[39] P. Azaria, H. T. Diep, and H. Giacomini, Phys. Rev. Lett. **59**, 1629 (1987).

[40] Y. Zhao, W. Li, B. Xi, Z. Zhang, X. Yan, S.-J. Ran, T. Liu, and G. Su, Phys. Rev. E **87**, 032151 (2013).

[41] I. A. Zaliznyak, C. Broholm, M. Kibune, M. Nohara, and H. Takagi, Phys. Rev. Lett. **83**, 5370 (1999).

[42] R. J. Vasconcelos dos Santos, I. P. Fittipaldi, P. Alstrøm, and H. E. Stanley, Phys. Rev. B **40**, 4527 (1989).

[43] M. L. Lyra and S. B. Cavalcanti, Phys. Rev. B **45**, 8021 (1992).

[44] M. L. Lyra and C. R. da Silva, Phys. Rev. B **47**, 526 (1993).

[45] V. J. Emery and G. Reiter, Phys. Rev. B **38**, 4547 (1988).

[46] R. J. Birgeneau, M. A. Kastner, and A. Aharony, Z. Phys. B: Condens. Matter **71**, 57 (1988).

[47] D. Vaknin, S. K. Sinha, D. E. Moncton, D. C. Johnston, J. M. Newsam, C. R. Safinya, and H. E. King, Phys. Rev. Lett. **58**, 2802 (1987).

[48] R. J. Birgeneau, C. Y. Chen, D. R. Gabbe, H. P. Jenssen, M. A. Kastner, C. J. Peters, P. J. Picone, T. Thio, T. R. Thurston, H. L. Tuller, J. D. Axe, P. Böni, and G. Shirane, Phys. Rev. Lett. **59**, 1329 (1987).

[49] A. Aharony, R. J. Birgeneau, A. Coniglio, M. A. Kastner, and H. E. Stanley, Phys. Rev. Lett. **60**, 1330 (1988).

[50] H. Alloul, J. Bobroff, M. Gabay, and P. J. Hirschfeld, Rev. Mod. Phys. **81**, 45 (2009).

[51] Q. Wang, C. Lin, Y. Ni, and Y. Zhang, J. Appl. Phys. **85**, 6061 (1999).

[52] Y. Itoh, N. Watanabe, S. Adachi, and T. Machi, Phys. C (Amsterdam, Neth.) **468**, 1234 (2008).

[53] K. Karmakar, A. Singh, S. Singh, A. Poole, and C. Rüegg, Cryst. Growth Des. **14**, 1184 (2014).

[54] K. Karmakar, R. Bag, and S. Singh, Cryst. Growth Des. **15**, 4843 (2015).

[55] I. A. Zaliznyak, H. Woo, T. G. Perring, C. L. Broholm, C. D. Frost, and H. Takagi, Phys. Rev. Lett. **93**, 087202 (2004).

[56] G. Simutis, S. Gvasaliya, M. Månsson, A. L. Chernyshev, A. Mohan, S. Singh, C. Hess, A. T. Savici, A. I. Kolesnikov, A. Piovano, T. Perring, I. Zaliznyak, B. Büchner, and A. Zheludev, Phys. Rev. Lett. **111**, 067204 (2013).

[57] T. Dietl, Nat. Mater. **9**, 965 (2010).

[58] H. Ohno, D. Chiba, F. Matsukura, T. Omiya, E. Abe, T. Dietl, Y. Ohno, and K. Ohtani, Nature (London) **408**, 944 (2000).

[59] D. Chiba, M. Sawicki, Y. Nishitani, Y. Nakatani, F. Matsukura, and H. Ohno, Nature (London) **455**, 515 (2008).

[60] C. Gould, C. Rüster, T. Jungwirth, E. Girgis, G. M. Schott, R. Giraud, K. Brunner, G. Schmidt, and L. W. Molenkamp, Phys. Rev. Lett. **93**, 117203 (2004).

[61] L. Mañosa, A. Planes, and M. Acet, J. Mater. Chem. A **1**, 4925 (2013).

[62] S. Manni, Y. Tokiwa, and P. Gegenwart, Phys. Rev. B **89**, 241102(R) (2014).

[63] A. Shadrin and Y. Panov, J. Magn. Magn. Mater. **546**, 168804 (2022).

[64] M. Ito, K. Onda, R. Kashima, A. Matsuo, and K. Kindo, J. Magn. Magn. Mater. **546**, 168767 (2022).

[65] M. E. Zhitomirsky, Phys. Rev. B **67**, 104421 (2003).

[66] M. E. Zhitomirsky and A. Honecker, J. Stat. Mech.: Theory Exp. (2004) P07012.

[67] M. S. S. Pereira, F. A. B. F. de Moura, and M. L. Lyra, Phys. Rev. B **79**, 054427 (2009).

[68] E. Warburg, Ann. Phys. (Berlin, Ger.) **249**, 141 (1881).

[69] P. Weiss and A. Piccard, J. Phys. Theor. Appl. **7**, 103 (1917).

[70] K. Synoradzki, J. Magn. Magn. Mater. **546**, 168857 (2022).

[71] K. A. Gschneidner and V. K. Pecharsky Jr., Annu. Rev. Mater. Sci. **30**, 387 (2000).

[72] B. G. Shen, J. R. Sun, F. X. Hu, H. W. Zhang, and Z. H. Cheng, Adv. Mater. **21**, 4545 (2009).

[73] S. Ghosh, A. Ghosh, P. Sen, and K. Mandal, Phys. Rev. Appl. **14**, 014016 (2020).

[74] V. K. Pecharsky and K. A. Gschneidner, Jr., Phys. Rev. Lett. **78**, 4494 (1997).

[75] A. Giguère, M. Foldeaki, B. Ravi Gopal, R. Chahine, T. K. Bose, A. Frydman, and J. A. Barclay, Phys. Rev. Lett. **83**, 2262 (1999).

[76] O. Tegus, E. Brück, K. H. J. Buschow, and F. R. de Boer, Nature (London) **415**, 150 (2002).

[77] P. J. von Ranke, N. A. de Oliveira, B. P. Alho, E. J. R. Plaza, V. S. R. de Sousa, L. Caron, and M. S. Reis, J. Phys.: Condens. Matter **21**, 056004 (2009).

[78] P. von Ranke, B. P. Alho, E. Nóbrega, and N. de Oliveira, Phys. B (Amsterdam, Neth.) **404**, 3045 (2009).

[79] J. M. Florez, P. Vargas, C. Garcia, and C. A. Ross, J. Phys.: Condens. Matter **25**, 226004 (2013).

[80] K. Szałowski and T. Balcerzak, J. Phys.: Condens. Matter **26**, 386003 (2014).

[81] T. Liu, X.-Y. Liu, Y. Gao, H. Jin, J. He, X.-L. Sheng, W. Jin, Z. Chen, and W. Li, Phys. Rev. Res. **3**, 033094 (2021).

[82] M. Keskin and M. Ertaş, Phys. Rev. E **80**, 061140 (2009).

[83] I. Diaz and N. Branco, Phys. A (Amsterdam, Neth.) **468**, 158 (2017).

[84] P. Xu and A. Du, Phys. B (Amsterdam, Neth.) **521**, 134 (2017).

[85] L. Gálisová and D. Jakubczyk, Phys. A (Amsterdam, Neth.) **466**, 30 (2017).

[86] Y. Panov, Phys. Rev. E **106**, 054111 (2022).